Optik - International Journal for Light and Electron Optics 266 (2022) 169648

Contents lists available at ScienceDirect

Optik

journal homepage: www.elsevier.com/locate/ijleo

A 1060 nm stretched-pulse mode-locked wavelength-swept laser source providing an A-scan rate of 20 MHz

Ibrahim Akkaya [a,b], Serhat Tozburun [a,c,d,*]

[a] Izmir Biomedicine and Genome Center, 35340 Balcova, Türkiye
[b] Department of Electrical and Electronics Engineering, Faculty of Engineering, Ege University, 35040 Bornova, Türkiye
[c] Izmir International Biomedicine and Genome Institute, Dokuz Eylul University, 35340 Balcova, Türkiye
[d] Department of Biophysics, Faculty of Medicine, Dokuz Eylul University, 35340 Balcova, Türkiye

ARTICLE INFO

Keywords:
Chromatic dispersion
Lasers
Optical coherence tomography
Wavelength tunning

ABSTRACT

The laser source is the deciding factor in improving the rapid imaging of swept-source optical coherence tomography (OCT) systems. We introduce an intrinsically stable stretched-pulse mode-locking (SPML) laser operating a tuning range of over 92 nm at a center wavelength of 1060 nm. The laser provides variable A-line rates up to ~20 MHz as a function of the duty cycle. The cavity comprises a unidirectional ring cavity with matched positive and negative continuously chirped fiber Bragg gratings generating ± 556 ps/nm dispersion. We demonstrate the ability of the stretched-pulse mode-locking laser to provide rapid optical signals for optical coherence tomography. Finally, we highlight performance by displaying the 3D datasets acquired at > 19,487 × 10^3 A-lines/s as cross-sectional images, averaging the complex A-scan signals of the voxel, and examining the inter-frame phase variance without the need for trigger signals and a phase calibration method. By integrating three-dimensional coherence-based optical imaging into a video-rate, camera-like deployment using a high-speed digitizer, this laser may potentially leverage the use of optical coherence tomography of complex tissue dynamics in pre-clinical studies

1. Introduction

Four-dimensional (i.e., adding time to function) and high-resolution imaging of biological tissues can be critical in developing technologies and approaches for scientific studies and clinical applications. In this sense, Fourier-domain Optical Coherence Tomography [1,2] has accompanied innovations in elastography [3], intraoperative [4], endoscopic [5], and angiographic [6] techniques and applications. In addition, various wavelength-swept laser source designs and OCT systems [7] that provide rapid imaging have been presented with the studies conducted in this context. The dispersion tuning and pulse stretching are two of the approaches developed for wavelength-swept lasers [8–11]. These laser approaches provide passive wavelength-selective filtering in the laser cavity. It has reached the point of producing tens of Megahertz A-line repetition rates with high sensitivity for high quality and fast OCT imaging with a mode-locking technique [7]. For example, we previously demonstrated stretched-pulse mode-locked (SPML) lasers at 1.55 μm [12] and 1.29 μm [13] center wavelengths. An OCT system based on SPML has been introduced that offers rapid and phase stable measurements for Doppler analysis between frames at ~24 kHz and volumes at 100 Hz [14]. Another SPML laser [15] with theta cavity design using a more complex electrical gating sequence with a single chromatic dispersion element in the laser cavity produced a

* Corresponding author at: Izmir Biomedicine and Genome Center, 35340 Balcova, Türkiye.
E-mail address: serhat.tozburun@deu.edu.tr (S. Tozburun).

https://doi.org/10.1016/j.ijleo.2022.169648
Received 2 May 2022; Received in revised form 24 June 2022; Accepted 12 July 2022
Available online 14 July 2022

sweep at a central wavelength of 1.3 μm for OCT [16]. However, reducing the central wavelength of the laser from the telecommunication wavelength range to a shorter laser wavelength could leverage this intrinsically phase-stable and rapid platform to broader clinical applications [17].

In this paper, we extend the stretched-pulsed mode-locked laser technology by providing a sweeping range of 92 nm centered at 1060 nm. As a result, the laser allows a variable repetition rate of up to ~20 MHz with a 100% duty cycle for rapid OCT. Additionally, the dispersion-based sweep and actively modulated cavity loss according to the cavity round trip time sufficiently increase the sensitivity making the laser suitable for use in OCT. The performance of the laser for phase-sensitive imaging is investigated by performing inter-frame phase variance analysis on a capillary phantom while oversampling A-line signals. The paper is organized into four sections, including the introduction. Section 2 presents the laser configuration and results regarding the performance of the laser. Section 3 begins with a description of the balanced Michelson interferometer setup. Next, we detail the preliminary OCT performances of the SPML laser at 1.06 μm. Finally, Section 4 discusses the current limitations of the study and summarizes the paper.

2. Materials and methods

2.1. Configuration of SPML laser

Fig. 1 shows the schematic of the unidirectional ring-cavity laser. A 10-GHz lithium-niobate intensity modulator (NIR-MX-LN-10, iXblue Photonics, France) with an extinction ratio of up to 30 dB generated broadband optical pulses. The modulator had an insertion loss of 4.9 dB at the maximum transmission. A bias controller (MBC-DG-LAB, iXblue Photonics, France) was locked to the modulator to compensate for any drift and maintain a high optical pulse contrast value and stability. A bit pattern generator (PAT5000, Sympuls, Germany) driven the modulator with short electrical pulses (<0.30 ns full width at half-maximum). Besides, an RF signal generator (SG386, Stanford Research System, USA) clocked the pattern generator externally for low timing noise and jitter. The electrical pulses were synchronized to a harmonic of the cavity round trip time for active mode-locking.

Rapid wavelength sweeping can be achieved using a frequency-dependent intracavity optical component that ensures a large chromatic dispersion. To have a constant cavity round-trip time throughout the optical frequency range to be swept, another optical component with opposite dispersion matches the chromatic dispersion to high order in the cavity. Two customized chirped fiber Bragg gratings (chirped-FBG, Proximion Fiber Systems, Sweden) used for this purpose provided highly matched dispersion of ± 556 ps/nm at 1060 nm and were incorporated into the cavity via wide-band circulators (Precision Micro-Optics, USA). The peak-to-peak group delay ripple (GDR) was only < 40 ps over the 92 nm wavelength interval. In the present configuration, the negative chirped-FBG stretched optical pulses with a pulse width of < 300 ps to 51.3 ns, and then the positive compressed them into the initial shape produced by the optical modulator.

We used optical amplifiers based on semiconductor technology as the gain medium to produce a broad optical spectrum in the 1-μm wavelength range with high saturation output power. The two optical amplifiers were cascaded to overcome non-uniform insertion loss throughout the tuning range caused by customized FBGs. Specifically, the insertion loss of the negative chirped-FBG was higher at a short wavelength (5.5-dB loss at 1020 nm) than a long wavelength (3.5-dB loss at 1100 nm). Thus, it contributed to improving the intensity noise level while enabling the laser to scan at total bandwidth. One of the amplifiers (SOA 1060, Innolume, Germany) emitted a 92 nm bandwidth centered at 1.06 μm, while the booster (BOA1050P, Thorlabs, USA) had a dominant emission between 1015 nm and 1060 nm. We have integrated an optical isolator (PMOI-1064-SS, Innolume, Germany) between the optical amplifiers to prevent unwanted back-emission and allow unidirectional operation of the laser.

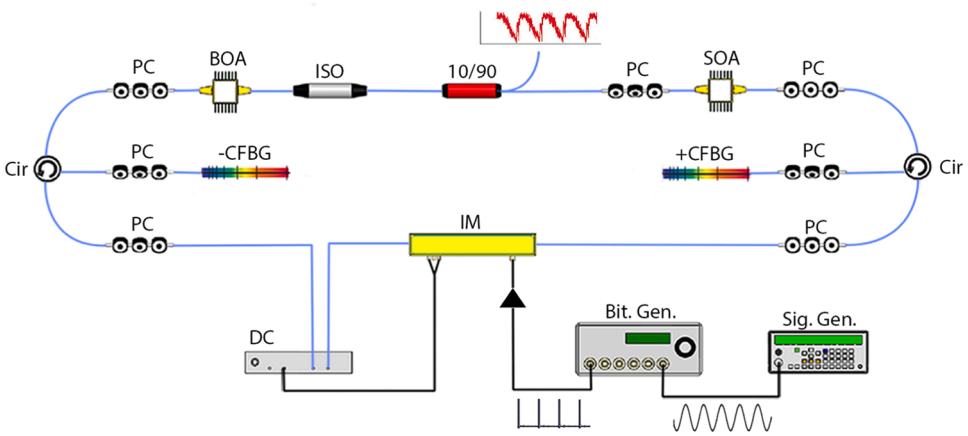

Fig. 1. A schematic of the stretched-pulse mode-locked laser. BOA: booster optical amplifier; CFBG: chirped fiber Bragg grating (± 556 ps/nm at 1060 nm); Circ: circulator; DC: bias controller; IM: intensity modulator; ISO: isolator; PC: polarization controlling pedal; SOA: semiconductor optical amplifier.

2.2. Laser performance

Fig. 2(a) and (b) show the time-domain laser outputs of compressed and stretched pulses detected with a 25 GHz bandwidth photodetector (UPD-15-IR2-FC, Alphalas, Germany). Up to 40 GS/s oscilloscope (DPO7354C, Tektronix, USA) digitalized analog signals. The laser was operated at a pulse repetition rate of > 19.4 MHz with a 100% duty cycle, corresponding to the fourth order harmonic of the laser cavity. Fig. 2(c) shows the typical spectral output produced by the laser. Chirped-FBGs, the modulator, and amplifiers were highly dependent on the polarization state of the light as they are highly polarization-sensitive optical components. Therefore, manual three-bladed (i.e., quarter-wave plate, half-wave plate, and quarter-wave plate in series) controllers were employed in the cavity to align the polarization state in terms of maximum transmission and gain. The measured lasing bandwidth was > 92 nm. It was determined that a combination of inconstant insertion loss and polarization mode distribution caused by chirped-FBGs throughout the scanning range limits this bandwidth. The measured average output power of the SPML laser was 52.8 mW using a 10/90 (10% output) output coupler (TW1064R2A2A, Thorlabs, USA). To characterize the measure of relative fluctuations in output power over time, we determined the relative intensity noise (RIN) of the laser in the 2 GHz range by subtracting the shot noise power and receiver noise (thermal noise) from the detected RIN. As shown in Fig. 2(d), the RIN of the laser was estimated to be a value of − 119.27 dB/Hz at 598.2 MHz.

3. Results

The value of an OCT image in characterizing laser source performance was appreciated. However, the inherently high (effectively ~20 MHz A-line speed) speed of the source required a GS/s digitizer with the required high bit depth. This section characterizes acquired point spread functions (PSFs) and demonstrated OCT imaging using a high-speed (10 GS/s, 3.5 GHz) oscilloscope with limited memory.

3.1. Interferometer and microscope

Fig. 3 shows a schematic representation of a fiber-based balanced Michelson interferometer used as an imaging engine to examine the laser's performance further. A wavelength combiner (W635S415A1A, Thorlabs, USA) mixed the SPML source with a red (635 nm) aiming beam to align the invisible laser beam with the sample before transmitting it to the interferometer. The interferometer consisted of fiber couplers (TW1064R5A2A, Thorlabs, USA) at a ratio of 50/50. The laser beam was split into a sample arm (50%) and a reference arm (50%). The coupler transmitted the backscattered light collected from the sample and the other 50/50 recombined with the reference arm to the photodetector in two equal proportions.

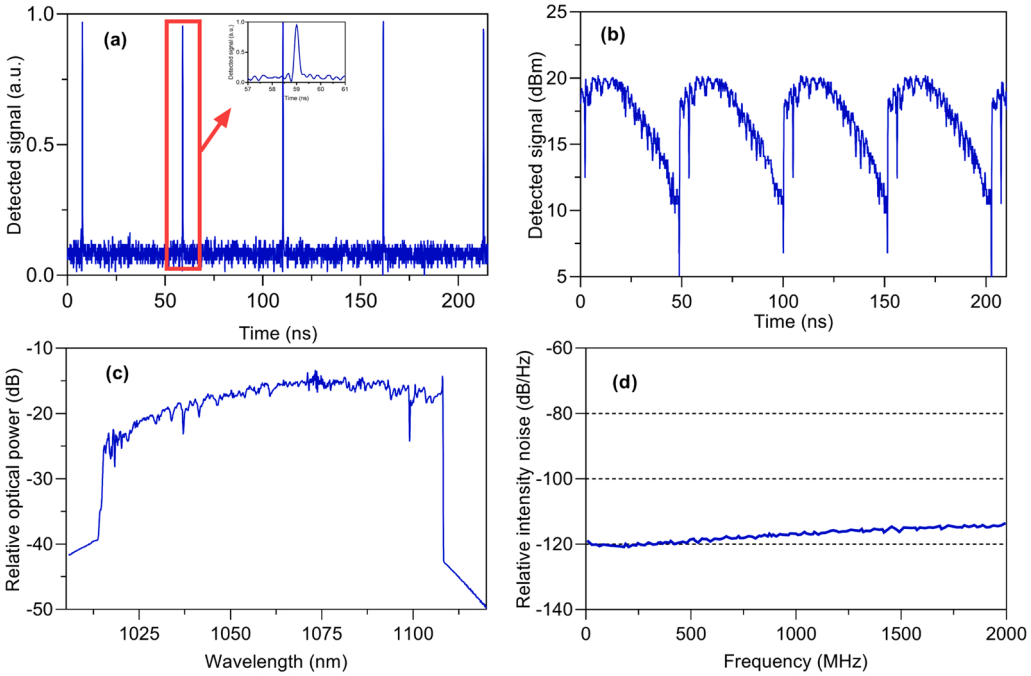

Fig. 2. The measured outputs of the SPML laser. Compressed (a) and stretched (b) laser outputs in the time domain at ~20 MHz repetition rate with a duty cycle of close to 100%. (c) The lasing spectrum is > 92 nm at the center wavelength of 1060 nm. (d) The relative intensity noise (RIN) of the SPML laser across the 2 GHz spectral range.

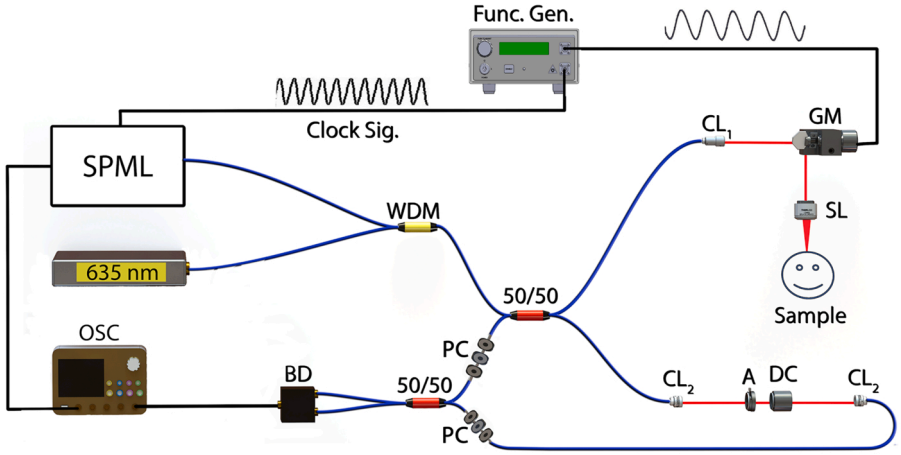

Fig. 3. A schematic of the balanced Michelson interferometer. A. aperture; BD: balanced photodetector (1.6 GHz); CL_1: collimator (f = 18.2 mm); CL_2: collimator (f = 4.56 mm); DC: dispersion compensator; GM: galvo scanner; OSC: Oscilloscope (~10 GS/s); PC: polarization controlling pedal; SL: scanning lens; WDM: wavelength-division multiplexer.

The sample arm included a collimator, an 18 mm focal length scan imaging lens (LSM-02-BB, Thorlabs, USA), and a 1D Galvo scanner (Compact 506, Scanner Max, USA). Collimated light with a ~3.8 mm beam diameter was launched to the scanner with a 4 mm window size. The lateral resolution was estimated to be ~10.5 μm on the sample with a scanning range of 4.5 mm. Dispersion mismatch between sample and reference arms due to double pass through the scanning lens was minimized by using two anti-reflective coated, bulk glass compensators (LSM02DC, Thorlabs, USA). A continuously variable iris diaphragm was used in the reference arm to optimize the signal-to-noise ratio by adjusting the beam diameter in free space.

A balanced photodetector (PDB480C-AC, Thorlabs, USA) combined with the 3.5-GHz bandwidth oscilloscope acquired fringe signals as a function of the interferometer delay. The oscilloscope also included memory (125 M points) that stores digitized signals generated by the system. The imaging depth range was limited to > 900 μm in tissue due to RF acquisition bandwidth limitations. The power of the scanning light at the sample was 18.4 mW.

An RF signal generator (SG384, Stanford Research System, USA) produced master clock signals. The laser, oscilloscope, and scanner driver (i.e., a function generator) were locked to a master clock. The frequencies were set as integer multiples of each other to intrinsically produce phase-stable fringes. The RF generator externally clocked the bit generator at 4.988754236 GHz and provided a clock signal to the oscilloscope at a sampling rate of 10 GHz. The phase-locked function generator drove the scanners to produce ~20,000 A-scans at 974.366061 Hz. A total of 513 samples were acquired per A-scan at the 19.48732123 MHz sweep rate.

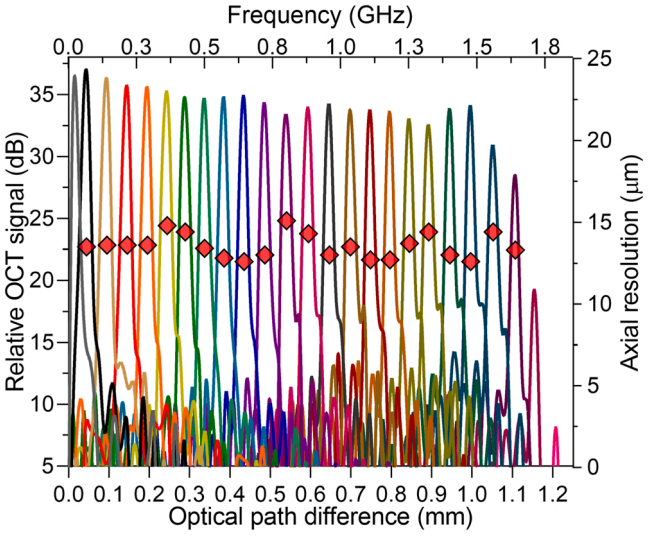

Fig. 4. Point spread functions measurements for multiple mirror distances in the air. The axial resolution was measured to be > 12.5 μm at the mirror distance of 0.1 mm.

3.2. OCT performance

First, we estimated the point spread functions (PSFs) for multiple mirror distances. As shown in Fig. 4, the fringe amplitude decay indicated a drop to approximately 6 dB of its path-matched value at > 0.95 mm. The measured axial resolution (FWHM of point spread functions) in the air was determined to be > 12.5 μm at a distance of 0.1 mm in a double-pass sample arm configuration. The resolution did not significantly vary (12–15 μm) within 1.1 mm mirror displacement. On the other hand, it has been noted that windowing can result in an effective FWHM laser bandwidth of 44 nm and deteriorate the measured axial resolution down to 21.8 μm.

For the fringe measurement, a gold-coated mirror was aligned to the sample arm, and then a neutral density filter with an optical

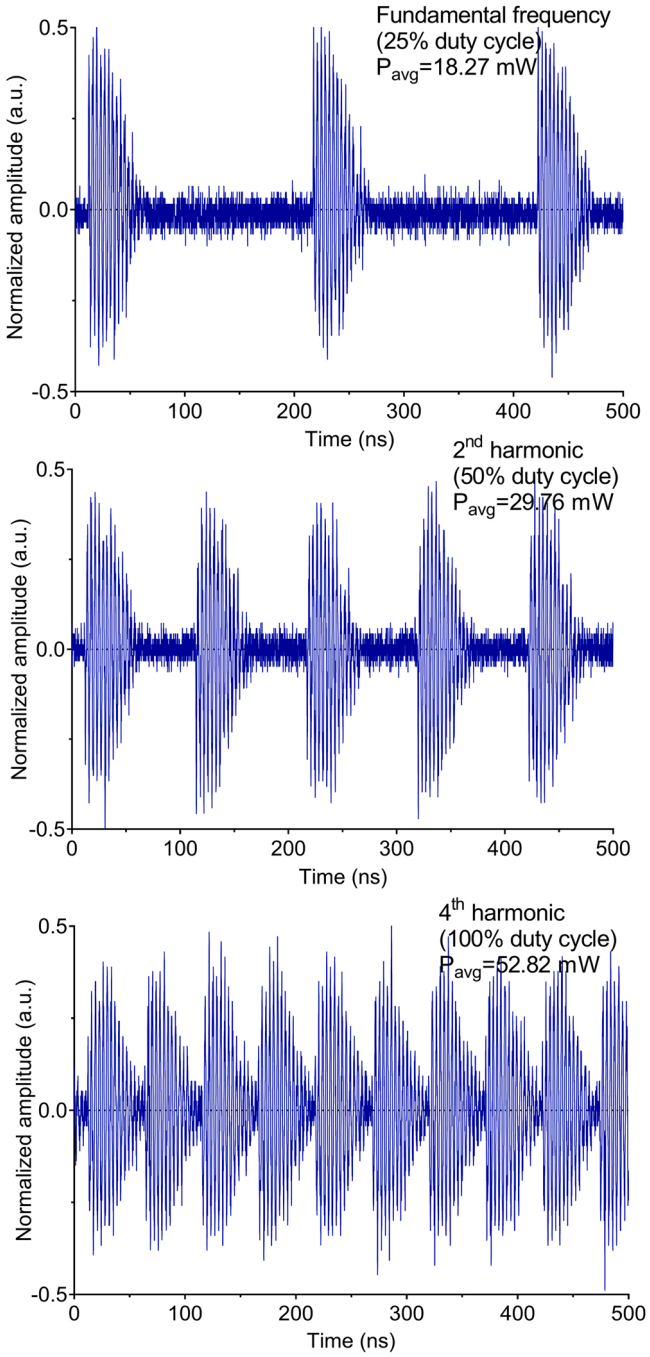

Fig. 5. Interference signals generated by the laser operating at 25%, 50%, and 100% duty cycle, respectively. The corresponding average output power is measured to be 18.3 m W, 29.8 mW, and 52.8 mW.

density of 2.0 (introducing 40-dB attenuation in double-pass configuration) was placed in front of the mirror to mimic optical loss of the biological sample. A 1.6 GHz balanced photodetector measured the fringe signals up to the bandwidth limit corresponding to < 1.1 mm double-pass mirror displacement.

Our previous study [12] noted that the pulse width of the optical pulses generated by the modulator mainly defines the coherence length in this laser design. Narrower optical pulses produced greater wavelength separation, thus increasing the coherence length. Nevertheless, narrowing pulse width reduced the stability due to likely interplays between pulse width and relaxation time of the SOA (on the order of 100 ps). To have a more stable laser in the RF bandwidth (1.6 GHz) limited PSF measurement, we operated the laser with a slightly reduced coherence length (slightly higher electrical pulse width driving the intensity modulator). The linewidth of the electrical pulses was < 300 ps.

Next, we investigated fringe signals at fixed mirror distance as a function of cavity frequency harmonics. The laser cavity length was 42.468 m, and the fundamental frequency was about 4.9 MHz. Fig. 5 shows the signals generated by the laser operating at the repetition rate of 4.88 MHz (25% duty cycle), 9.75 MHz (50% duty cycle), and 19.49 MHz (100% duty cycle), respectively. According to the working principle of the laser operating in a harmonic resonant mode, the product of the lasing bandwidth and the dispersion limits the sweep rate, independent of the overall cavity round trip time. Therefore, the laser can be operated at a 100% duty cycle with minor fine-tuning to the laser cavity length, considering the overall distribution matching in the cavity.

The standard deviation of the measured phase difference between the adjacent A line was calculated as $\pm$ 70 mrad. According to the model in Ref. [18], the estimated standard deviation corresponded to a phase noise from the 26 dB signal.

Finally, some cross-sectional images produced by the SPML laser at 1.06 μm are given as an example to demonstrate the imaging capability of the laser in the current data acquisition system (i.e., a fast oscilloscope). The resulting 3D raw dataset size was $513 \times 20{,}000 \times 4$ and was processed in Matlab (Mathworks, USA). Conventional post-data processing was performed, including a zero-padded fast Fourier transformation on each A-scan to decrease the axial-data array size from 513 to 220. Spline interpolation linearly rescaled the volumetric dataset to remove the sinusoidal driving waveform in the scan-axis. Also, only forward scanning of the scanner was used. The complex A-lines were first grouped in sets of 10, coherently averaged to improve the signal-to-noise ratio. Thus, the final complex 3D datasets were in the size of 110 by 1000 by 4. The logged amplitude and phase information of each pixel was extracted from the complex data and stored separately on an 8-bit scale for further processing. The average incident power on the sample surface was decreased to 1.95 mW at 1060.3 nm, considering the American National Standards Institute (ANSI) limit of < 2.0 mW.

This study used 0.75 mm outer diameter capillaries as a sample, shown in Fig. 6(a). These 0.5 mm inner diameter capillaries (0.75 mm outer diameter) were filled with milk for contrast. The surface was scanned in a single axis, at a frame rate of 974.4 Hz, over 4.5 mm, based on a focal length of 18 mm. The logarithmic intensity scaling for structural OCT image construction was performed. Fig. 6(b) shows a cross-sectional view of the capillaries with an imaging depth of approximately 500 μm due to the RF bandwidth limit and complex conjugate ambiguity. Capillaries of different heights were placed at a distance of approximately 2.0 mm from end to end. The height difference between the capillary tubes was calculated as approximately 144 μm. Note the gap (i.e., wall of the tube) between the outer surface of the capillary tube and the milk-filled inner surface.

Next, the phase difference between coherently averaged A-lines was calculated to provide phase contrast information over time. We then explored the inter-frame variance of the phase difference over consecutively acquired B-scans (i.e., phase difference variance data relative to the adjacent frame, $\Delta\varphi(x,y,t_{i+1}) - \Delta\varphi(x,y,t_i)$). Fig. 6(c) illustrates an extracted inter-frame phase variance cross-sectional view. Due to the effective suppression of phase difference variance in static data over time [19], the method contrasted the surface of the capillary tube with the surrounding air and the milk-filled interior with the glass wall of the tube. Besides, Fig. 6(c) presents that the system provides a high degree of phase coherence between successive B-scans (frames) over several milliseconds (limited by memory) without requiring A-line trigger signals or implementation of post-processing phase calibration algorithms. This phase coherence was achieved by the inherent stability of the SPML design, which employs phase-locked electronics to drive the optical modulator, scanner, and oscilloscope.

4. Discussion and conclusions

This study demonstrates a stretched-pulse active mode-locked (SPML) laser at the center wavelength of 1.06 μm. The laser provides a repetition rate of ~20 MHz over a 92 nm wavelength range for rapid OCT imaging. The high A-line scan rate allows for an OCT imaging at >MHz while increasing the SNR using coherent averaging. Besides, we highlight the possible interests of the laser's ability to provide phase-sensitive imaging in a phantom without the need for k-clocking, A-line triggers, or phase calibration methods.

This article reveals several limitations that are beyond its scope and should be discussed in future studies. First, we plan to improve the effective polarization control in the cavity to avoid polarization-induced loss and polarization mode dispersion caused by chirped-FBGs written on standard single-mode fibers [20]. Second, although the measured coherence length < 1 mm seems rather low considering current demands, the measurement is limited by the bandwidth of the balanced detector (1.6 GHz) used in the study. The coherence length provided by the laser can be examined with a larger bandwidth photodetector. Third, the essence of further investigation of the OCT capabilities of the laser on a biological sample is noted. For this purpose, the laser source in its current form requires a high-speed data acquisition card coupled with a large amount of random-access memory. Finally, apart from the chirped-FBGs, the fiber components forming the laser cavity caused a dispersion of about $-$ 0.8 ps/nm. This relatively low dispersion, which was ignored in this study, can be eliminated by adding a compensator to the cavity.

With a high-speed digitizer that can transmit long data sequences acquired in tens of seconds, the laser may have significant potential in pre-clinical ophthalmology studies.

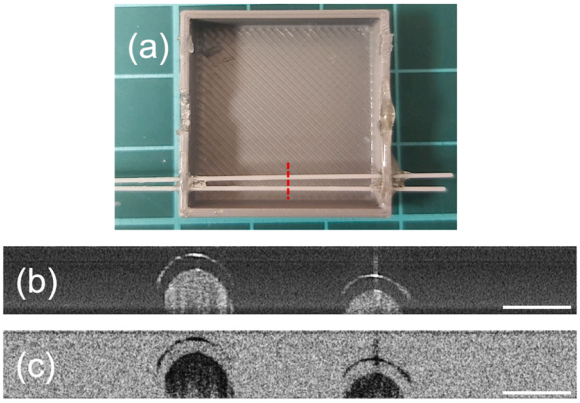

Fig. 6. (a) Milk-filled capillaries with an outer diameter of 0.75 mm were used as samples. Cross-sectional amplitude (b) and inter-frame phase variance (c) images were obtained from the sample. Coherent averaging was performed in sets of 10 A-lines to improve the signal-to-noise ratio. Scale bar = 500 μm.

Funding

This work was supported partially by the Scientific and Technological Research Institution of Türkiye (TUBITAK) grant no. 116F192 and the Turkish Academy of Sciences Young Scientists Award Programme (2018 TUBA-GEBIP).

CRediT authorship contribution statement

Ibrahim Akkaya: Investigation, building the system, planning, and executing all experiments, and preparing the figures. **Serhat Tozburun**: Obtaining support, Conceptualization, Investigation, Writing – original draft.

Declaration of Competing Interest

The authors declare that they have no known competing financial interests or personal relationships that could have appeared to influence the work reported in this paper.

Data availability

Data will be made available on request.

Acknowledgements

The authors gratefully acknowledge support and thank Hanife Gokkan at Dokuz Eylul University for her help in generating some figures.

References

[1] S. Yun, G. Tearney, J. de Boer, N. Iftimia, B. Bouma, High-speed optical frequency-domain imaging, Opt. Express 11 (22) (2003) 2953–2963.
[2] M. Choma, M. Sarunic, C. Yang, J. Izatt, Sensitivity advantage of swept source and Fourier domain optical coherence tomography, Opt. Express 11 (18) (2003) 2183–2189.
[3] V. Larin, D.D. Sampson, Optical coherence elastography – OCT at work in tissue biomechanics [Invited], Biomed. Opt. Express 8 (2) (2017) 1172–1202.
[4] O.M. Carrasco-Zevallos, C. Viehland, B. Keller, M. Draelos, A.N. Kuo, C.A. Toth, J.A. Izatt, Review of intraoperative optical coherence tomography: technology and applications [Invited], Biomed. Opt. Express 8 (3) (2017) 1607–1637.
[5] M.J. Gora, M.J. Suter, G.J. Tearney, X. Li, Endoscopic optical coherence tomography: technologies and clinical applications [Invited], Biomed. Opt. Express 8 (5) (2017) 2405–2444.
[6] C.-L. Chen, R.K. Wang, Optical coherence tomography based angiography, Biomed. Opt. Express 8 (2) (2017) 1056–1082.
[7] T. Klein, R. Huber, High-speed OCT light sources and systems [Invited], Biomed. Opt. Express 8 (2) (2017) 828–859.
[8] S. Yamashita, Dispersion-tuned swept lasers for optical coherence tomography, IEEE J. Sel. Top. Quantum Electron. 24 (3) (2018). Art. no. 6800109.
[9] X. Wei, C. Kong, G.K. Samanta, K.K. Tsia, K.K.Y. Wong, Self-healing highly-chirped fiber laser at 1.0 μm, Opt. Express 24 (24) (2016) 27577–27586.
[10] J. Xu, X. Wei, L. Yu, C. Zhang, J. Xu, K.K.Y. Wong, K.K. Tsia, High-performance multi-megahertz optical coherence tomography based on amplified optical time-stretch, Biomed. Opt. Express 6 (4) (2015) 1340–1350.
[11] H.D. Lee, G.H. Kim, J.G. Shin, Akinetic swept-source optical coherence tomography based on a pulse-modulated active mode locking fiber laser for human retinal imaging, Sci. Rep. 8 (2018). Art. no. 17660.
[12] S. Tozburun, M. Siddiqui, B.J. Vakoc, A rapid, dispersion-based wavelength-stepped and wavelength-swept laser for optical coherence tomography, Opt. Express 22 (3) (2014) 3414–3424.
[13] I. Akkaya, S. Tozburun, An 18.6 MHz wavelength-swept laser source based on stretched-pulse mode-locking at 1290 nm, in: European Conferences on Biomedical Optics 2021 (ECBO), OSA Technical Digest (Optical Society of America, 2021), Art. no. ETu3D.6.

[14] S. Tozburun, C. Blatter, M. Siddiqui, E.F.J. Meijer, B.J. Vakoc, Phase-stable Doppler OCT at 19 MHz using a stretched-pulse mode-locked laser, Biomed. Opt. Express 9 (3) (2018) 952–961.
[15] R. Khazaeinezhad, M. Siddiqui, B.J. Vakoc, 16 MHz wavelength-swept and wavelength-stepped laser architectures based on stretched-pulse active mode locking with a single continuously chirped fiber Bragg grating, Opt. Lett. 42 (10) (2017) 2046–2049.
[16] T.S. Kim, J.Y. Joo, I. Shin, P. Shin, W.J. Kang, B.J. Vakoc, W.Y. Oh, 9.4 MHz A-line rate optical coherence tomography at 1300 nm using a wavelength-swept laser based on stretched-pulse active mode-locking, Sci. Rep. 10 (2020). Art. no. 9328.
[17] O.M. Carrasco-Zevallos, C. Viehland, B. Keller, M. Draelos, A.N. Kuo, C.A. Toth, J.A. Izatt, Review of intraoperative optical coherence tomography: technology and applications [Invited], Biomed. Opt. Express 8 (3) (2017) 1607–1637.
[18] B.H. Park, M.C. Pierce, B. Cense, S.H. Yun, M. Mujat, G.J. Tearney, B.E. Bouma, J.F. de Boer, Realtime fiber-based multi-functional spectral-domain optical coherence tomography at 1.3 μm, Opt. Express 13 (11) (2005) 3931–3944.
[19] J. Fingler, D. Schwartz, C. Yang, S.E. Fraser, Mobility and transverse flow visualization using phase variance contrast with spectral domain optical coherence tomography, Opt. Express 15 (20) (2007) 12636–12653.
[20] J. Joo, T.S. Kim, B.J. Vakoc, W. Oh, Robust and easy-to-operate stretched-pulse mode-locked wavelength-swept laser with an all-polarization-maintaining fiber cavity for 10 MHz A-line rate optical coherence tomography, Opt. Lett. 46 (16) (2021) 3857–3860.